Quantum shortcut to adiabaticity for state preparation in a finite-sized Jaynes-Cummings lattice

Kang Cai, Prabin Parajuli, Anuvetha Govindarajan, and Lin Tian*
School of Natural Sciences, University of California, Merced, Merced, California 95343, USA

(Received 19 February 2024; revised 12 July 2024; accepted 14 August 2024; published 26 August 2024; corrected 2 April 2025)

In noisy quantum systems, achieving high-fidelity state preparation using the adiabatic approach faces a dilemma: either extending the evolution time to reduce diabatic transitions or shortening it to mitigate decoherence effects. Here we present a quantum shortcut to adiabaticity for state preparation in a finite-sized Jaynes-Cummings lattice by applying counterdiabatic (CD) driving along given adiabatic trajectories. Leveraging the symmetry of eigenstates in our system, we convert the CD driving to an implementable Hamiltonian that only involves local qubit-cavity couplings for a two-site lattice with one polariton excitation. Additionally, we derive a partial analytical form of the CD driving for the lattice with two excitations. Our numerical results demonstrate that circuit errors and environmental noise have negligible effects on our scheme under practical parameters. We also show that our scheme can be characterized through the detection of qubit operators. This approach can lead to a promising pathway to high-fidelity state preparation in a significantly reduced timescale when compared to conventional adiabatic methods.

DOI: 10.1103/PhysRevA.110.022621

I. INTRODUCTION

Adiabatic evolution involves a gradual transformation of a quantum system from an initial state to a desired final state by slowly varying a time-dependent Hamiltonian and has been extensively studied for quantum state preparation in quantum information processing [1,2]. In noisy quantum systems [3,4], achieving high fidelity for the prepared states using the adiabatic approach requires a balance in choosing the evolution time: It should be long enough to reduce unwanted diabatic transitions yet short enough to mitigate decoherence from environmental noise. Various approaches have been used to develop a quantum shortcut to adiabaticity, where reverse engineering of diabatic transitions is employed to accelerate a slow adiabatic process via nonadiabatic shortcuts [5–8]. These approaches include counterdiabatic (CD) driving [9–13], invariant-based approaches [14,15], the derivative removal of an adiabatic gate [16], dressed-state approaches [17], etc. The quantum shortcut to adiabaticity has been proposed and experimentally demonstrated in many quantum systems, such as superconducting qubits, defect qubits, quantum-dot arrays, and cold atoms [18–30]. One hurdle that prevents the general application of these quantum shortcut approaches is the complexity of the Hamiltonian required for reverse engineering, which often involves multipartite or nonlocal interactions. A number of approaches have been explored to overcome this hurdle by deriving local CD driving, including an approach that explores the self-similar nature of a quantum system, the mean-field approximation, a variational approach, Floquet engineering, a digitalized approach, and an optimal control approach [31–40].

Jaynes-Cummings (JC) lattices [41–49] have been studied in various experimental systems, including superconducting qubits coupled to cavities, solid-state defects coupled to nanocavities, and trapped ions [50–57], and can exhibit quantum or dissipative phase transitions between the Mott-insulating and superfluid phases in the thermodynamic limit [47,48,58,59]. The states of finite-sized JC lattices can also carry related features, resulting in novel phenomena such as the photon blockade effect and novel entanglement when properly populated with polariton excitations [60,61]. A key step in demonstrating these effects is to prepare the desired quantum states with a finite number of excitations. In previous works we employed an adiabatic approach and a quantum optimal control approach for state preparation in this system [62,63].

Here we present a quantum shortcut to adiabaticity for state preparation in a finite-sized JC lattice by applying CD driving during an adiabatic evolution. In our approach we explore the symmetry of the system's eigenstates to convert the CD driving to an implementable Hamiltonian for two-site and three-site lattices. We find that for a two-site lattice with one excitation, the CD driving can involve only local qubit-cavity couplings, and with two excitations, the CD driving can have a partial analytical form that involves four-operator couplings in the antisymmetric subspace. We also study the effects of control errors and environmental noise on our scheme, which complements previous CD driving studies on noisy and open quantum systems [36,64,65]. Our numerical results demonstrate that the effects of circuit errors and environmental noise are negligible under practical parameters. Meanwhile, this scheme can be characterized by performing measurement on the qubits. This work hence presents an implementable CD driving that can greatly shorten the evolution time of an adiabatic process in a JC lattice and provides a promising avenue

*Contact author: ltian@ucmerced.edu

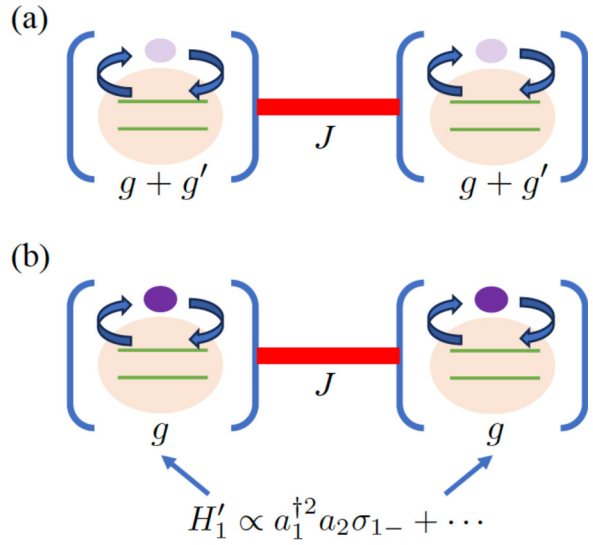

FIG. 1. Schematic of a two-site JC lattice with (a) one polariton excitation and (b) two polariton excitations. Each site is composed of a qubit (two-level system) coupled to a cavity mode with coupling strength g and the cavities are connected by photon hopping with rate J. The CD driving (a) includes only local qubit-cavity couplings denoted by g' and (b) is shown as H_1'.

to achieving high-fidelity state preparation in a significantly reduced timescale.

II. JAYNES-CUMMINGS LATTICE

Consider a finite-sized JC lattice composed of JC models coupled via photon hopping between adjacent sites, as illustrated in Fig. 1. The Hamiltonian of the JC lattice can be written as $H_{\rm JC} = H_0 + gV_g + JV_J$, where $H_0 = \sum_j(\omega_0 a_j^\dagger a_j + \frac{\omega_z}{2}\sigma_{jz})$ is the Hamiltonian of the uncoupled qubits and cavity modes, $V_g = \sum_j(a_j^\dagger\sigma_{j-} + \sigma_{j+}a_j)$ describes the on-site qubit-cavity coupling, and $V_J = -\sum_j(a_i^\dagger a_{i+1} + a_{i+1}^\dagger a_i)$ describes the photon hopping between neighboring sites. Here a_j ($a_j^\dagger$) is the annihilation (creation) operator of the cavity modes, $\sigma_{j\pm}$ and σ_{jz} are the Pauli operators of the qubits, ω_0 is the frequency of the cavities, ω_z is the qubit energy splitting, g is the strength of the qubit-cavity coupling, J is the photon hopping rate, and $j \in [1, N]$, with N the number of sites. We have assumed $\hbar = 1$ for convenience of discussion. In the rotating frame defined by $H_0^{\rm rot} = \omega_z\sum_j(a_j^\dagger a_j + \frac{1}{2}\sigma_{jz})$, the Hamiltonian of the JC lattice becomes $H_{\rm r} = \sum_j \Delta a_j^\dagger a_j + gV_g + JV_J$, where $\Delta = \omega_0 - \omega_z$ is the detuning between the cavity modes and the qubits.

We denote the basis states of a single JC model by $|n, s\rangle$, with $n \geqslant 0$ the photon number of the cavity mode and $s = g, e$ the ground and excited states of the qubit, respectively. The eigenstates of a single JC model include the ground state $|0, g\rangle$ and the doublets $|n, \pm\rangle$ ($n \geqslant 1$), which are superpositions of the basis states $|n, g\rangle$ and $|n-1, e\rangle$ and correspond to eigenstates with n polariton excitations. In the thermodynamic limit with $N \to \infty$, a JC lattice can exhibit various many-body effects such as the quantum and dissipative phase transitions between the Mott insulating and the superfluid phases [41–43]. It can be shown that the ground states of a finite-sized JC lattice exhibit similar features to these phases [47,62,63].

A key step in studying novel phenomena in a JC lattice is the preparation of desired quantum states for a finite number of polariton excitations. One approach to generate such states is adiabatic evolution [62], where the system is first prepared in the ground state of an initial Hamiltonian $H_{\rm r}(t_0)$ at time t_0, followed by adiabatic tuning of the system parameters to reach the target Hamiltonian $H_{\rm r}(T)$ at the final time T. The ground state of the target Hamiltonian is designed to be the desired state, which is often hard to prepare directly by gate operations. In the end of the adiabatic evolution, the system will reach the desired state. However, the adiabaticity of the evolution and hence the fidelity of the prepared states can be impaired by unwanted diabatic transitions to excited states. Below we will employ a quantum shortcut to adiabaticity approach to study the robust generation of quantum states in a JC lattice within a significantly reduced time frame.

III. COUNTERDIABATIC DRIVING

Counterdiabatic driving can be applied to the Hamiltonian $H_{\rm r}(t)$ to cancel diabatic transitions and generate quantum shortcut to adiabaticity during an adiabatic evolution. The CD driving has the general form [5,9,10]

$$H_1(t) = i\sum_{m\neq n}\frac{|m(t)\rangle\langle m(t)|\partial_t H_{\rm r}|n(t)\rangle\langle n(t)|}{E_n(t) - E_m(t)}, \tag{1}$$

where $|m\rangle$ and $|n\rangle$ are instantaneous eigenstates of $H_{\rm r}(t)$ at time t, and E_m and E_n are the corresponding eigenenergies. The total Hamiltonian of this system then becomes $H_{\rm tot} = H_{\rm r}(t) + H_1(t)$. The exact CD Hamiltonian in (1) often includes nonlocal or multipartite interactions due to the complexity of the quantum system of interest. Hence, it is challenging to implement this Hamiltonian in systems with practical parameters.

In this section we convert the CD driving in (1) to an implementable Hamiltonian for adiabatic evolutions in two-site and three-site JC lattices. Our results show that the CD driving can comprise only local qubit-cavity couplings and is implementable using current technology.

A. Two sites with one excitation

1. Eigenstates

We first study a two-site JC lattice with only one polariton excitation. The allowable Hilbert space for this system includes four basis states $|1, g\rangle_1|0, g\rangle_2$, $|0, e\rangle_1|0, g\rangle_2$, $|0, g\rangle_1|1, g\rangle_2$, and $|0, g\rangle_1|0, e\rangle_2$, where the subscripts refer to sites 1 and 2 in the lattice. Written in terms of this basis set, the Hamiltonian has the form

$$H_{\rm r} = \begin{pmatrix} \Delta & g & -J & 0 \\ g & 0 & 0 & 0 \\ -J & 0 & \Delta & g \\ 0 & 0 & g & 0 \end{pmatrix} \tag{2}$$

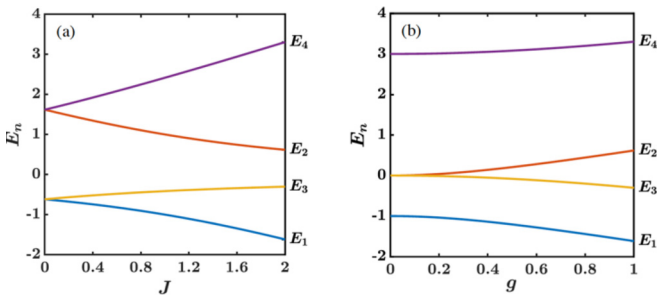

FIG. 2. Eigenenergies E_n ($n \in [1, 4]$) of a two-site JC lattice with one excitation. (a) E_n vs hopping rate J for $g = 1$ and $\Delta = 1$. (b) E_n vs coupling constant g for $J = 2$ and $\Delta = 1$. All parameters are in dimensionless units.

for given values of g, J, and Δ. The eigenvalues E_n ($n \in [1, 4]$) of this system are

$$E_{1,2} = \tfrac{1}{2}(\Delta_J^- \mp \chi_1^-), \quad E_{3,4} = \tfrac{1}{2}(\Delta_J^+ \mp \chi_1^+), \tag{3}$$

with $\Delta_J^\pm = \Delta \pm J$ and $\chi_1^\pm = \sqrt{(\Delta_J^\pm)^2 + 4g^2}$. The corresponding eigenvectors are

$$v_1 = \tfrac{1}{2}\begin{pmatrix} -\sqrt{\frac{\chi_1^- - \Delta_J^-}{\chi_1^-}} \\ \sqrt{\frac{\chi_1^- + \Delta_J^-}{\chi_1^-}} \\ -\sqrt{\frac{\chi_1^- - \Delta_J^-}{\chi_1^-}} \\ \sqrt{\frac{\chi_1^- + \Delta_J^-}{\chi_1^-}} \end{pmatrix}, \quad v_2 = \tfrac{1}{2}\begin{pmatrix} \sqrt{\frac{\chi_1^- + \Delta_J^-}{\chi_1^-}} \\ \sqrt{\frac{\chi_1^- - \Delta_J^-}{\chi_1^-}} \\ \sqrt{\frac{\chi_1^- + \Delta_J^-}{\chi_1^-}} \\ \sqrt{\frac{\chi_1^- - \Delta_J^-}{\chi_1^-}} \end{pmatrix},$$

$$v_3 = \tfrac{1}{2}\begin{pmatrix} \sqrt{\frac{\chi_1^+ - \Delta_J^+}{\chi_1^+}} \\ -\sqrt{\frac{\chi_1^+ + \Delta_J^+}{\chi_1^+}} \\ -\sqrt{\frac{\chi_1^+ - \Delta_J^+}{\chi_1^+}} \\ \sqrt{\frac{\chi_1^+ + \Delta_J^+}{\chi_1^+}} \end{pmatrix}, \quad v_4 = \tfrac{1}{2}\begin{pmatrix} -\sqrt{\frac{\chi_1^+ + \Delta_J^+}{\chi_1^+}} \\ -\sqrt{\frac{\chi_1^+ - \Delta_J^+}{\chi_1^+}} \\ \sqrt{\frac{\chi_1^+ + \Delta_J^+}{\chi_1^+}} \\ \sqrt{\frac{\chi_1^+ - \Delta_J^+}{\chi_1^+}} \end{pmatrix}. \tag{4}$$

The eigenstate v_1 is the ground state with eigenenergy E_1. From (4) we observe that the states v_1 and v_2 are symmetric with respect to the exchange of the states on the two sites, while the states v_3 and v_4 are antisymmetric and acquire a factor of -1 when the states on the two sites are swapped. In Fig. 2(a) we plot the energy spectrum of the system as a function of the photon hopping rate J for $g = 1$ and $\Delta = 1$. At $J = 0$, $\Delta_J^\pm = \Delta$, resulting in $E_1 = E_3$ ($E_2 = E_4$), which indicates that the states v_1 and v_3 (v_2 and v_4) are degenerate. In Fig. 2(b) we plot the energy spectrum vs the qubit-cavity coupling g for $J = 2$ and $\Delta = 1$. At $g = 0$ and $\Delta < J$, $E_2 = E_3 = 0$, and v_2 and v_3 are degenerate.

We want to emphasize that the symmetry of these eigenstates is crucial for our development of an implementable CD driving that only involves local qubit-cavity couplings. During an adiabatic evolution, the variation of the Hamiltonian does not induce transition of the system from a symmetric to an antisymmetric state due to the inherent symmetry of the Hamiltonian. Furthermore, this symmetry also facilitates the preparation of the ground state v_1 at $J = 0$ via resonant pumping, without inducing excitation to the state v_3 that is degenerate to v_1.

2. *Ramping of hopping rate J*

We assume that the hopping rate $J(t)$ is continuously tuned from $J(0) = 0$ at time $t = 0$ to $J(T) = J_f$ at the final time T, with J_f the target hopping rate, while keeping the qubit-cavity coupling and the detuning unchanged during the adiabatic process. At $t = 0$, the system is prepared in the ground state v_1 for $J = 0$ by resonantly pumping the system from the state $|0, g\rangle_1|0, g\rangle_2$. The variation of $J(t)$ induces off-diagonal matrix elements between the instantaneous eigenstates, resulting in undesired transitions to the excited states. The nonzero matrix elements are $|\langle v_1|V_J|v_2\rangle| = g/\chi_1^-$ and $|\langle v_3|V_J|v_4\rangle| = g/\chi_1^+$, along with their conjugate elements, which induce transitions between the states v_1 and v_2 and between the states v_3 and v_4, respectively. We then derive the CD driving using (1):

$$H_1(t) = i\frac{g}{(\chi_1^-)^2}\frac{dJ}{dt}(|v_1\rangle\langle v_2| - |v_2\rangle\langle v_1|) - i\frac{g}{(\chi_1^+)^2}\frac{dJ}{dt}(|v_3\rangle\langle v_4| - |v_4\rangle\langle v_3|). \tag{5}$$

Hence, when the system is in the ground state v_1, the only allowable transition is to the symmetric eigenstate v_2. As discussed above, this is due to the symmetry of the eigenstates and the Hamiltonian. A variation of the hopping rate in the Hamiltonian preserves the exchange symmetry of the state, which can only induce a diabatic transition to the state v_2. Consequently, the state at an arbitrary time t during the evolution remains symmetric and can only be a superposition of the instantaneous v_1 and v_2 states. Thus, the second term in $H_1(t)$ does not actively contribute to the elimination of diabatic transitions and its amplitude can be adjusted with flexibility, without affecting the adiabatic dynamics of this system. Below we will construct an easier-to-implement CD driving using this property.

We first convert the CD driving in (5) to physical operators of the qubits and cavities to see if it can be easily implemented. In the Hilbert space for one polariton excitation, we have $a_1^\dagger\sigma_{1-} = |1, g\rangle_1\langle 0, e| \otimes |0, g\rangle_2\langle 0, g|$, $a_1^\dagger a_2 = |1, g\rangle_1\langle 0, g| \otimes |0, g\rangle_2\langle 1, g|$, and so forth. Using the expression of the eigenstates in (4), we derive

$$|v_1\rangle\langle v_2| - |v_2\rangle\langle v_1| = \tfrac{1}{2}(S_+^\dagger A_+ - A_+^\dagger S_+), \tag{6a}$$

$$|v_3\rangle\langle v_4| - |v_4\rangle\langle v_3| = \tfrac{1}{2}(S_-^\dagger A_- - A_-^\dagger S_-), \tag{6b}$$

with $A_\pm = a_1 \pm a_2$ and $S_\pm = \sigma_{1-} \pm \sigma_{2-}$. In addition, the CD driving Hamiltonian can be written as

$$H_1(t) = i\frac{g}{2(\chi_1^-)^2}\frac{dJ}{dt}(S_+^\dagger A_+ - A_+^\dagger S_+) - i\frac{g}{2(\chi_1^+)^2}\frac{dJ}{dt}(S_-^\dagger A_- - A_-^\dagger S_-). \tag{7}$$

This Hamiltonian comprises local couplings between qubits and cavities on the same site such as $\sigma_{1+}a_1$ and $\sigma_{2+}a_2$ as well as nonlocal couplings between qubits and neighboring cavities such as $\sigma_{1+}a_2$ and $\sigma_{2+}a_1$.

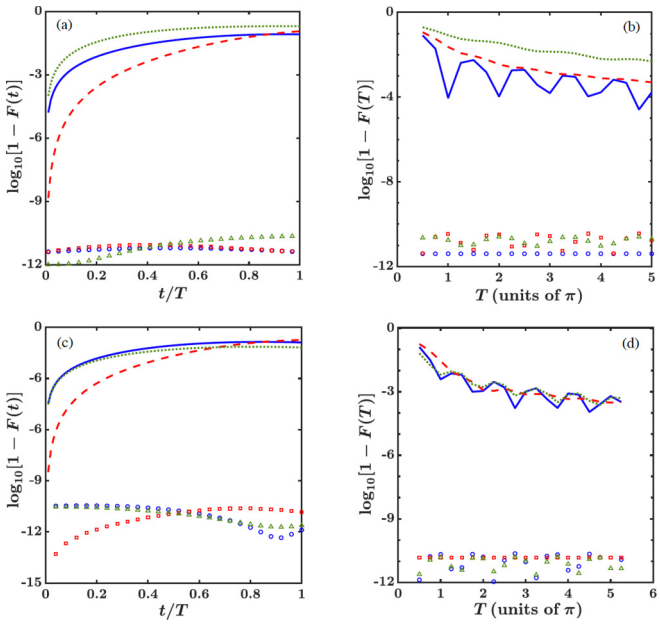

FIG. 3. Infidelity $1-F(t)$ vs t/T for a total evolution time of $T=0.5\pi$ for (a) two-site and (c) three-site JC lattices and infidelity $1-F(T)$ vs T for (b) two-site and (d) three-site JC lattices. In all plots, the blue solid line (blue circles) denotes the linear ramping of hopping rate J for $g\equiv 1$, $\Delta\equiv 1$, $J(0)=0$, and $J_f=2$ under the adiabatic Hamiltonian $H_{\rm r}$ only (with the CD driving H_1' applied); red dashed line (red squares), quadratic ramping of J for $g\equiv 1$, $\Delta\equiv 1$, $J(0)=0$, and $J_f=2$ under $H_{\rm r}$ (with H_1'); and green dotted line (green triangles), linear ramping of coupling g for $J\equiv 2$, $\Delta\equiv 1$, $g(0)=0$, and $g_f=1$ under $H_{\rm r}$ (with H_1'). All parameters are in dimensionless units.

By changing the coefficient of the second term in (7) from $-ig/2(\chi_1^+)^2$ to $ig/2(\chi_1^-)^2$, we obtain the following CD Hamiltonian:

$$H_1'(t)=ig'(a_1\sigma_{1+}-a_1^\dagger\sigma_{1-}+a_2\sigma_{2+}-a_2^\dagger\sigma_{2-}). \tag{8}$$

This Hamiltonian includes only local qubit-cavity couplings with coupling strength given by $g'=\frac{g}{(\chi_1^-)^2}\frac{dJ}{dt}$. It can be interpreted as a Jaynes-Cummings coupling with an $e^{i\pi/2}$ phase and can be implemented by adjusting local qubit-cavity couplings.

For demonstration, we simulate the time evolution of this system under the adiabatic Hamiltonian $H_{\rm r}$ with either H_1 or H_1' applied. We consider both linear ramping of the hopping rate with $J(t)=J_f\frac{t}{T}$ and quadratic ramping of the hopping rate with $J(t)=J_f(\frac{t}{T})^2$. For linear ramping, $dJ/dt=J_f/T$; for quadratic ramping, $dJ/dt=2J_ft/T^2$. We choose the target hopping rate $J_f=2$, the qubit-cavity coupling $g\equiv 1$, the detuning $\Delta\equiv 1$, and the total time $T=0.5\pi$. We define the fidelity of the quantum state at time t as $F(t)=|\langle v_1(t)|v(t)\rangle|^2$, where $v(t)$ is the state at time t and $v_1(t)$ is the instantaneous ground state of the adiabatic Hamiltonian at time t. In Fig. 3(a) we plot the infidelity $1-F(t)$ vs t/T. Without the CD driving, the infidelity increases significantly during the evolution, as the diabatic transitions can be serious for a very short evolution time of $T=0.5\pi$. In contrast, when the CD driving H_1' is applied, the infidelity, up to a small numerical error below 10^{-10}, is zero throughout the evolution and the system is preserved in the ground state. In Fig. 3(b) we plot the infidelity $1-F(T)$ of the final state vs the total evolution time T. Without the CD driving, the infidelity can be quite high for a short evolution time. This result demonstrates that the CD approach can ensure high fidelity for a short evolution time, which is crucial for devices in the noisy intermediate-scale quantum regime [3]. As shown in Figs. 7(a) and 7(b) in Appendix A, the infidelities under H_1 and H_1' are the same up to a small numerical error below 10^{-10}, which confirms our analysis that these two CD drivings yield the same dynamics for the initial state v_1.

3. Ramping of qubit-cavity coupling g

Now consider an adiabatic trajectory where the qubit-cavity coupling is ramped linearly with $g(t)=g_f\frac{t}{T}$, where g_f is the target coupling strength. The nonzero transition matrix elements caused by the variation of g are $|\langle v_1|V_g|v_2\rangle|=\Delta_J^-/\chi_1^-$, $|\langle v_3|V_g|v_4\rangle|=\Delta_J^+/\chi_1^+$, and their conjugate elements, which induce transitions between the states v_1 and v_2 as well as between the states v_3 and v_4, respectively, due to the symmetry of the eigenstates. The CD driving can be derived as

$$H_1(t)=i\frac{\Delta_J^-}{2(\chi_1^-)^2}\frac{dg}{dt}(S_+^\dagger A_+-A_+^\dagger S_+) -i\frac{\Delta_J^+}{2(\chi_1^+)^2}\frac{dg}{dt}(S_-^\dagger A_--A_-^\dagger S_-). \tag{9}$$

Similar to (7), this Hamiltonian includes nonlocal couplings between qubits and neighboring cavities. As discussed above, when $|v_1\rangle$ is the initial state, only the state $|v_2\rangle$ could be excited by diabatic transitions. Therefore, we can vary the coefficient of the second term in (9). By changing this coefficient from $-i\Delta_J^+/2(\chi_1^+)^2$ to $i\Delta_J^-/2(\chi_1^-)^2$, we obtain the CD driving

$$H_1'(t)=ig'(a_1\sigma_1^+-a_1^\dagger\sigma_1^-+a_2\sigma_2^+-a_2^\dagger\sigma_2^-), \tag{10}$$

which only involves local qubit-cavity couplings with strength $g'=\frac{\Delta_J^-}{(\chi_1^-)^2}\frac{dg}{dt}$. Consequently, implementing both the adiabatic Hamiltonian and the CD driving only requires the tuning of the local qubit-cavity coupling, which can significantly simplify the experimental setup.

We perform a numerical simulation on this system with a hopping rate of $J\equiv 2$, a detuning of $\Delta\equiv 1$, and a target coupling strength of $g_f=1$. At $t=0$ and $g(0)=0$, the initial state is $(|1,g\rangle_1|0,g\rangle_2+|0,g\rangle_1|1,g\rangle_2)/\sqrt{2}$, where the excitation is stored in the cavity modes. The infidelity $1-F(t)$ vs t/T for $T=0.5\pi$ is plotted in Fig. 3(a) and the infidelity at the final time $1-F(T)$ vs the total time T is plotted in Fig. 3(b). The results are similar to the case of ramping the hopping rate J.

4. Self-protected trajectory

The magnitude of the CD driving in (10) is proportional to $\Delta_J^-=\Delta-J$. In the special case of $\Delta=J$, $\Delta_J^-=0$, leading to the interesting result $H_1'=0$, which means that no CD driving is required. It can be shown that the matrix element $|\langle v_1|V_g|v_2\rangle|\equiv 0$ under this condition; hence the only

allowable diabatic transition for the initial state v_1 disappears. The Hamiltonian H_r is thus self-protected from the diabatic transition, i.e., there is no diabatic transition when ramping the qubit-cavity coupling g. The ground state is $\frac{1}{\sqrt{2}}(|1,-\rangle_1|0,g\rangle_2+|0,g\rangle_1|1,-\rangle_2)$ throughout the evolution, with the system occupying the lower polariton state $|1,-\rangle$ in one of the lattice sites.

B. Three sites with one excitation

We now study a three-site lattice with one polariton excitation under the open boundary condition with the photon hopping term $V_J=-(a_1^\dagger a_2+a_2^\dagger a_3+\text{H.c.})$, where sites 1 and 3 possess mirror reflection symmetry. The allowable Hilbert space comprises six basis states $|1,g\rangle_1|0,g\rangle_2|0,g\rangle_3$, $|0,e\rangle_1|0,g\rangle_2|0,g\rangle_3$, $|0,g\rangle_1|1,g\rangle_2|0,g\rangle_3$, $|0,g\rangle_1|0,e\rangle_2|0,g\rangle_3$, $|0,g\rangle_1|0,g\rangle_2|1,g\rangle_3$, and $|0,g\rangle_1|0,g\rangle_2|0,e\rangle_3$. The Hamiltonian in terms of this basis set has the form

$$H_r=\begin{pmatrix}\Delta & g & -J & 0 & 0 & 0\\ g & 0 & 0 & 0 & 0 & 0\\ -J & 0 & \Delta & g & -J & 0\\ 0 & 0 & g & 0 & 0 & 0\\ 0 & 0 & -J & 0 & \Delta & g\\ 0 & 0 & 0 & 0 & g & 0\end{pmatrix}. \tag{11}$$

We numerically calculate the eigenstates of this system. Four eigenstates exhibit symmetry regarding the exchange of the states on sites 1 and 3. For $g=1$, $J=2$, and $\Delta=1$, these symmetric states include the ground state v_1, the second excited state v_3, the third excited state v_4, and the highest state v_6. When ramping the hopping rate J, diabatic transitions occur only between v_1 and v_4 and between v_3 and v_6. Thus, the CD driving takes the form of $H_1=\alpha_1|v_4\rangle\langle v_1|+\alpha_2|v_6\rangle\langle v_3|+\text{H.c.}$ with coefficients α_1 and α_2. When expressed in terms of the physical operators, we have

$$\begin{aligned}H_1=&\,ig_n[(a_1^\dagger+a_3^\dagger)\sigma_{2-}+a_2^\dagger(\sigma_{1-}+\sigma_{3-})-\text{H.c.}]\\&+ig_l(a_1^\dagger\sigma_{3-}+a_3^\dagger\sigma_{1-}-\text{H.c.})\\&+ig_l(a_1^\dagger\sigma_{1-}+2a_2^\dagger\sigma_{2-}+a_3^\dagger\sigma_{3-}-\text{H.c.}),\end{aligned} \tag{12}$$

which includes nonlocal couplings with strengths g_n and g_l, such as the coupling between the cavities on sites 1 and 3 and the qubit on site 2, as well as local couplings with strength g_l for sites 1,3 and strength $2g_l$ for site 2.

We employ the same approach as in Sec. III A to convert the CD Hamiltonian to a form that is easier to implement. As discussed above, for the initial state v_1, ramping of the hopping terms only induces transition to the state v_4. Therefore, the coefficient α_2 in H_1 can be varied with flexibility without affecting the dynamics of this system. By adjusting α_2, we find

$$\begin{aligned}H_1'=&\,ig'(a_1^\dagger\sigma_{1-}+2a_2^\dagger\sigma_{2-}+a_3^\dagger\sigma_{3-}-\text{H.c.})\\&+ig'(a_1^\dagger\sigma_{3-}+a_3^\dagger\sigma_{1-}-\text{H.c.}),\end{aligned} \tag{13}$$

where the couplings between the qubit (cavity) on site 2 and the cavities (qubits) on sites 1 and 3 are no longer required. This Hamiltonian still includes nonlocal terms between sites 1 and 3 with coupling strength g'. This Hamiltonian can be implemented for a small lattice of three sites by coupling the qubits and cavities on sites 1 and 3. However, this result shows that we cannot always find a local form of the CD driving. In Figs. 3(c) and 3(d) we plot the infidelity of the prepared state under the adiabatic Hamiltonian H_r both without and with the CD driving H_1'. The result is similar to that of the two-site lattice discussed in Sec. III A.

C. Two sites with two excitations

1. Eigenstates

For a two-site JC lattice with two polariton excitations, the Hilbert space includes eight basis states $|2,g\rangle_1|0,g\rangle_2$, $|1,e\rangle_1|0,g\rangle_2$, $|0,g\rangle_1|2,g\rangle_2$, $|0,g\rangle_1|1,e\rangle_2$, $|1,g\rangle_1|1,g\rangle_2$, $|0,e\rangle_1|1,g\rangle_2$, $|1,g\rangle_1|0,e\rangle_2$, and $|0,e\rangle_1|0,e\rangle_2$. In the first four states, both excitations occupy one of the two sites, while in the last four states, one excitation is located on each site. Using this basis set, the Hamiltonian H_r can be expressed as

$$H_r=\begin{pmatrix}2\Delta & \sqrt{2}g & 0 & 0 & -\sqrt{2}J & 0 & 0 & 0\\ \sqrt{2}g & \Delta & 0 & 0 & 0 & -J & 0 & 0\\ 0 & 0 & 2\Delta & \sqrt{2}g & -\sqrt{2}J & 0 & 0 & 0\\ 0 & 0 & \sqrt{2}g & \Delta & 0 & 0 & -J & 0\\ -\sqrt{2}J & 0 & -\sqrt{2}J & 0 & 2\Delta & g & g & 0\\ 0 & -J & 0 & 0 & g & \Delta & 0 & g\\ 0 & 0 & 0 & -J & g & 0 & \Delta & g\\ 0 & 0 & 0 & 0 & 0 & g & g & 0\end{pmatrix}. \tag{14}$$

For detuning $\Delta=0$, the eigenvalues of this Hamiltonian can be derived analytically as

$$E_{1,2}=0, \tag{15a}$$

$$E_{3,4}=\mp\sqrt{2g^2+J^2}, \tag{15b}$$

$$E_{5,6}=\mp\frac{\sqrt{6g^2+5J^2-\sqrt{4g^4+60g^2J^2+9J^4}}}{\sqrt{2}}, \tag{15c}$$

$$E_{7,8}=\mp\frac{\sqrt{6g^2+5J^2+\sqrt{4g^4+60g^2J^2+9J^4}}}{\sqrt{2}}. \tag{15d}$$

In Fig. 4(a) we plot the eigenenergies vs the hopping rate J at $g=1$ and $\Delta=0$. We denote the eigenstates by v_i with $i\in[1,8]$, corresponding to the eigenvalues given in (15). Here v_7 is the ground state, while v_1 and v_2 are degenerate states with $E_{1,2}=0$.

2. Ramping of hopping rate J

Assuming that the hopping rate is linearly ramped with $J(t)=J_f\frac{t}{T}$, the target hopping rate $J_f=1$, $g\equiv1$, and $\Delta\equiv0$. The CD driving H_1 can be obtained numerically using Eq. (1). We simulate the dynamics of this system with the initial state being the ground state v_7 at $J=0$ for a total evolution time of $T=0.5\pi$. In Fig. 4(b) we plot the infidelity $1-F(t)$ of the

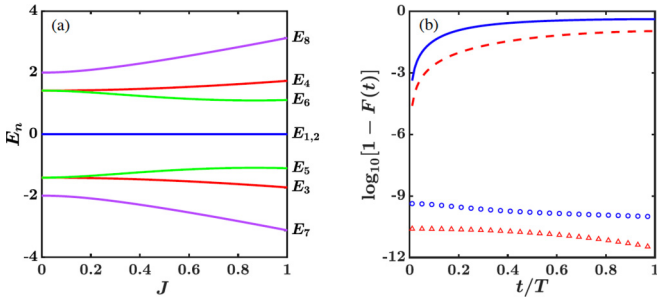

FIG. 4. (a) Eigenenergies E_n ($n \in [1, 8]$) vs hopping rate J. (b) Infidelity $1 - F(t)$ vs t/T for a total evolution time of $T = 0.5\pi$. The blue solid line (blue circles) denotes the linear ramping of hopping rate J under the adiabatic Hamiltonian H_r only (with the CD driving H_1 applied) with the initial state being the ground state v_7 at $J = 0$ and the red dashed line (red squares) the linear ramping of J under H_r (with H_1') with the initial state being the first excited state v_3 at $J = 0$. Here $g \equiv 1$, $\Delta \equiv 0$, $J(0) = 0$, $J_f = 1$, and all parameters are in dimensionless units.

quantum state at time t as a function of t/T. The infidelity at the final time T exceeds 0.4 under the adiabatic Hamiltonian H_r, whereas it remains negligible when the CD driving is applied.

By examining the eigenstates of H_r, we find that the eight eigenstates can be divided into two subsets. The first subset contains three states $\{v_2, v_3, v_4\}$, while the second subset contains the remaining five states, including the ground state v_7. When varying the hopping rate J, the only nonzero transition matrix elements are between states within the same subset and there is no diabatic transition between states in different subsets. Thus, for an initial state in the first subset, we consider the CD driving H_1' that only eliminates the diabatic transitions between eigenstates in this subset. As detailed in Appendix B, we derive

$$H_1'(t) = i\frac{g}{2(J^2+2g^2)}\frac{dJ}{dt}(A_2^\dagger C_2 - C_2^\dagger A_2), \tag{16}$$

where $A_2 = a_1^2 - a_2^2$ and $C_2 = a_2\sigma_{1-} - a_1\sigma_{2-}$. This Hamiltonian consists of four-operator terms, which can be formed through effective second-order couplings in the perturbative regime.

To demonstrate the effectiveness of Eq. (16), we conducted a numerical simulation of the adiabatic process on the initial state v_3 from the first subset, which corresponds to the first excited state in Fig. 4(a). As shown in Fig. 4(b), up to a small numerical error below 10^{-10}, the infidelity remains zero throughout the evolution, indicating that the diabatic transitions are completely canceled by the CD driving H_1'. In contrast, if the initial state is the ground state v_7 from the second subset, the infidelities both without and with the CD driving H_1' will be the same [see the blue solid line in Fig. 4(b)]. These numerical findings clearly show that the CD driving H_1' is only effective for states in the first subset, but not for states in the second subset, which is consistent with our analysis above.

IV. ERROR, NOISE, AND MEASUREMENT

In this section we discuss the effects of control errors and environmental noise on the adiabatic evolution under the CD driving, as well as the characterization of the CD approach through qubit measurements.

A. Control errors

Adjusting the system parameters can introduce classical control errors, potentially impacting the performance of the CD approach. To investigate the effects of these errors, we conducted numerical simulations of the adiabatic process by introducing random fluctuations to the time-dependent coupling constants. Consider the linear ramping of the hopping rate $J(t)$ discussed in Sec. III A, where the CD driving only consists of time-dependent local qubit-cavity couplings. We introduce a fluctuation $\delta J(t)$ to the hopping rate with $J(t) \to J(t) + \delta J(t)$ and a fluctuation $\delta g(t)$ to the qubit-cavity coupling [including the CD terms in (10)] with $g(t) \to g(t) + \delta g(t)$. Here $\delta J(t)$ and $\delta g(t)$ are Gaussian random numbers with standard deviations αJ_f and αg, respectively, where α is the ratio of the fluctuation amplitude to the coupling strength. We choose α to be below 0.15, i.e., the fluctuations are below 15% of the coupling strengths. In superconducting quantum devices, the couplings can be manipulated by various methods, as demonstrated in recent experiments [66–72], and the ratio α can be well below 5% [73].[1] In Fig. 5(a) the fidelity $F(t)$ is plotted vs t/T for a single sample of errors with $\alpha = 0.05$ and $T = 0.5\pi$. The fidelity exhibits small fluctuations over the time t due to the presence of the errors. In Fig. 5(b) the fidelity $F(T)$ averaged over 100 samples of errors is plotted vs the ratio α. As α increases to 15%, the fidelity only shows a mild decrease, demonstrating that control errors will not strongly affect the system dynamics in practical systems.

B. Decoherence

Environmental noise induces decoherence in the qubits and the cavity modes, potentially impacting the fidelity of the prepared quantum states. To analyze the effects of decoherence, we utilize a master equation approach with

$$\frac{d\rho}{dt} = -i[H_{\rm tot}, \rho] + \sum_j (\gamma_j \mathcal{L}_{qj} + \kappa_j \mathcal{L}_{aj})\rho, \tag{17}$$

where $\mathcal{L}_{qj} = \frac{1}{2}(2\sigma_{j-}\rho\sigma_{j+} - \rho\sigma_{j+}\sigma_{j-} - \sigma_{j+}\sigma_{j-}\rho)$ is the Liouvillian operator for the qubit on site j with damping rate γ_j, $\mathcal{L}_{aj} = \frac{1}{2}(2a_j\rho a_j^\dagger - \rho a_j^\dagger a_j - a_j^\dagger a_j\rho)$ is the Liouvillian operator for the cavity mode on site j with damping rate κ_j, and $H_{\rm tot}$ is the total Hamiltonian of the system. We choose

[1]For simplicity of discussion, we assume that the standard deviations of the circuit errors are αJ_f and αg, respectively, with the same ratio α. Under this assumption, the error amplitude is on the scale of a given percentage of the maximal hopping rate J_f or the coupling strength g, which is reasonable in practical devices. Meanwhile, for $J_f = 2$, $g = 1$, $\Delta = 1$, and $T \geqslant 0.5\pi$ ($dJ/dt = J_f/T$), the strength of the CD driving g' is on the same order as the magnitudes of g and J_f and hence will not introduce a large error beyond our assumption.

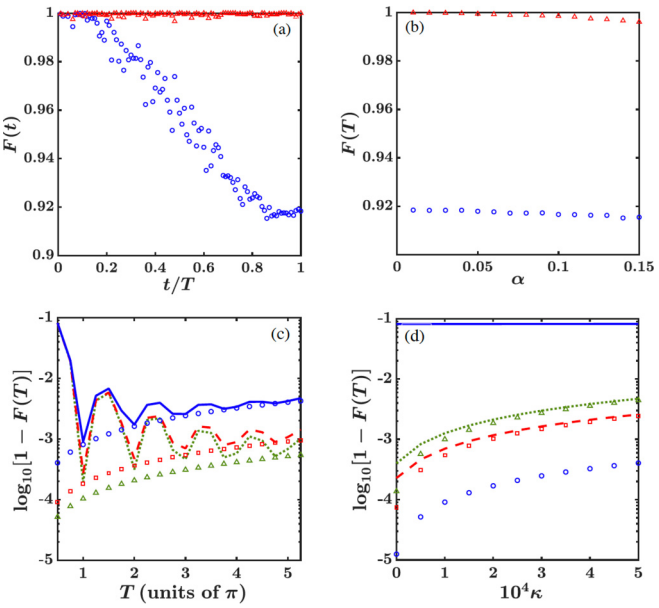

FIG. 5. (a) Fidelity $F(t)$ vs t/T for one sample of errors with $\alpha = 0.05$. (b) Fidelity $F(T)$ vs α averaged over 100 samples of errors. In (a) and (b) blue circles (red triangles) represent under the adiabatic Hamiltonian $H_{\rm r}$ only (with the CD driving H_1' applied) and the total evolution time is $T = 0.5\pi$. (c) Infidelity $1 - F(T)$ vs T for $\gamma = \frac{5}{\pi} \times 10^{-5}$. The blue solid line (blue circles) is for $\kappa = 5 \times 10^{-4}$ under the adiabatic Hamiltonian $H_{\rm r}$ only (with the CD driving H_1' applied), the red dashed line (red squares) is for $\kappa = 10^{-4}$ under $H_{\rm r}$ (with H_1'), and the green dotted line (green triangles) is for $\kappa = 5 \times 10^{-5}$ under $H_{\rm r}$ (with H_1'). (d) Infidelity $1 - F(T)$ vs κ for $\gamma = \frac{5}{\pi} \times 10^{-5}$. The blue solid line (blue circles) is for $T = 0.5\pi$ under the adiabatic Hamiltonian $H_{\rm r}$ only (with the CD driving H_1' applied), the red dashed line (red squares) is for $T = 3\pi$ under $H_{\rm r}$ (with H_1'), and the green dotted line (green triangles) is for $T = 5.5\pi$ under $H_{\rm r}$ (with H_1'). All plots are for linear ramping of hopping rate J with parameters given in Fig. 3 in dimensionless units.

$\gamma_{1,2} = \gamma$ and $\kappa_{1,2} = \kappa$ for simplicity of discussion. We also assume that the dimensionless coupling strength $g = 1$ in our discussion corresponds to $g = 2\pi \times 100$ MHz in superconducting systems [62,63]. The measured decoherence time of approximately 100 μs then corresponds to $\gamma = \frac{5}{\pi} \times 10^{-5}$ in dimensionless units. When the cavity frequency is $\omega_0 = 2\pi \times 5$ GHz and the quality factor is $Q = 10^6$, the cavity decay rate is $\kappa = 5 \times 10^{-5}$ in dimensionless units.

In Fig. 5(c) we plot the infidelity $1 - F(T)$ vs the total evolution time T for $\kappa = 5 \times 10^{-5}$, 10^{-4}, and 5×10^{-4}, with $\gamma = \frac{5}{\pi} \times 10^{-5}$. It can be seen that for a short evolution time $T = 0.5\pi$, the infidelity under only the adiabatic Hamiltonian is much larger than the infidelity with the CD driving H_1', indicating that the infidelity is dominated by diabatic transitions. In contrast, for a long evolution time $T = 5.5\pi$, the infidelities without and with the CD driving become comparable, indicating that it is dominated by the decoherence effect. In Fig. 5(d) we plot $1 - F(T)$ vs the cavity damping rate κ for $T = 0.5\pi$, 3π, and 5.5π. Here the infidelity increases slightly with κ for a short evolution time $T = 0.5\pi$, even when considering a decoherence rate much higher than the experimental value. In contrast, for a long evolution time such as $T = 5.5\pi$, the infidelity increases significantly with κ, indicating the dominance of the decoherence effect. This result clearly shows that by applying the implementable CD driving H_1', we can greatly reduce the decoherence effect by choosing a short evolution time and achieve high-fidelity quantum states. This finding confirms the effectiveness of the CD approach in mitigating the impact of decoherence. Meanwhile, as discussed in Sec. III A, the implementable CD driving H_1' generates the same system dynamics as the CD driving H_1 when the initial state is v_1. The effect of decoherence and circuit errors when H_1' is applied is hence the same as that when H_1 is applied. Using H_1' will not be more robust to noise and control errors than using H_1.

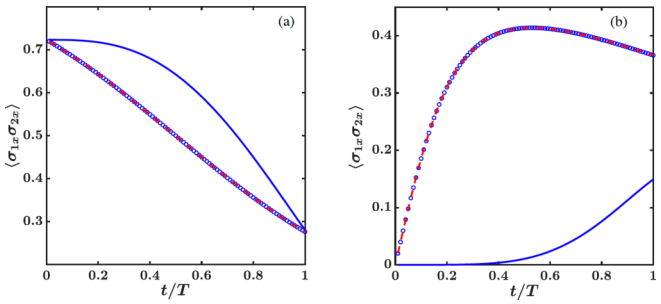

FIG. 6. Operator average $\langle\sigma_{1x}\sigma_{2x}\rangle$ vs t/T for $T = 0.5\pi$. (a) Two sites, one excitation with linear ramping of J and parameters given in Fig. 3 in dimensionless units. (b) Two sites, two excitations with linear ramping of J and parameters given in Fig. 4 in dimensionless units. In both plots the blue solid line (blue circles) represents under the adiabatic Hamiltonian $H_{\rm r}$ only (with the CD driving H_1' applied) and the red dashed line the instantaneous ground-state average of $H_{\rm r}$.

C. Measurement

The performance of the CD approach can be characterized by conducting measurement on the qubit operator $\sigma_{1x}\sigma_{2x}$. In the case of one excitation in a two-site lattice, the ground state at the initial parameters $g = 1$, $J = 0$, and $\Delta = 1$ is $\frac{1}{2}(|1,-\rangle_1|0,g\rangle_2 + |0,g\rangle_1|1,-\rangle_2)$, where $|1,-\rangle$ is the lower polariton state with one excitation, and the excitation occupies the sites in the form of a quantum superposition with the operator average $\langle\sigma_{1x}\sigma_{2x}\rangle = 0.7236$. When the hopping rate becomes $J_f = 2$ at time T, the operator average of the ground state decreases to $\langle\sigma_{1x}\sigma_{2x}\rangle = 0.2764$, as shown in Fig. 6(a). It is noticeable that the operator average for the adiabatic evolution under $H_{\rm r}$ can significantly deviate from that of the ground state, while the operator average with the CD driving applied remains the same as that of the ground state. Similarly, in the two-excitation case, the ground state at $g = 1$, $J = 0$, and $\Delta = 0$ is $v_7 = |1,-\rangle_1|1,-\rangle_2$, where each site is occupied by one excitation in the lower polariton state with the operator average $\langle\sigma_{1x}\sigma_{2x}\rangle = 0$. When the hopping rate becomes $J_f = 1$, the operator average increases to $\langle\sigma_{1x}\sigma_{2x}\rangle = 0.3659$. During the evolution, the operator average for the adiabatic process without the CD driving shows a large discrepancy from the operator average in the CD approach, as shown in Fig. 6(b). Hence, the effectiveness of the CD approach can be verified by measuring the operator average.

V. CONCLUSION

We have studied a quantum shortcut to adiabaticity using the counterdiabatic driving approach in a finite-sized JC lattice, leveraging the symmetry inherent in its eigenstates. Our analysis reveals that for a two-site lattice with one excitation, the CD driving can be simplified to a realizable form that only consists of local qubit-cavity couplings. For more complex scenarios, such as a two-site lattice with two excitations or a three-site lattice with one excitation, a simpler CD Hamiltonian can still be obtained, albeit involving nonlocal terms. Our numerical simulations demonstrate that control errors and environmental noise have negligible effects on our scheme in practical systems and our scheme can be characterized through measurements on the qubits. Overall, our findings offer a promising avenue for achieving high-fidelity quantum state preparation and hold potential for applications across various systems exhibiting similar symmetries.

ACKNOWLEDGMENTS

This work was supported by the NSF Award No. DMR-2037987 and the UC-MRPI Program (Grant No. M23PL5936). A.G. was also supported by the Sandbox AQ Fellowship.

APPENDIX A: RELATION BETWEEN H_1 AND H_1'

In Sec. III A our analysis showed that the system dynamics under the CD driving H_1' will be exactly the same as that of the CD driving H_1, when the initial state is v_1. In Figs. 3(a) and 3(b) we plotted the infidelity for a two-site lattice with one excitation under the CD driving H_1', where the infidelity remains zero up to a small numerical error below 10^{-10}. In Figs. 7(a) and 7(b) we plot the infidelity of this system under both H_1 and H_1' for a linear ramping of the hopping rate J using the same parameters as given in Figs. 3(a) and 3(b). It can be clearly seen that the infidelities for both H_1 and H_1' remain zero up to the numerical error, which confirms our analysis.

Furthermore, we compare the effect of the CD drivings H_1 and H_1' by numerically calculating two quantities: (i) the average energy of the system $E_{\text{ave}} = \langle v(t)|H_{\text{tot}}(t)|v(t)\rangle$ at time t, with H_{tot} the total Hamiltonian and $v(t)$ the instantaneous wave function, and (ii) the energy cost $\Delta E = E_{\text{ave}} - E_G$, with E_G the instantaneous ground-state energy at time t following the definition in [74]. In Fig. 7(c) we plot E_{ave} for linear ramping of the hopping rate J on the initial state $|v_1\rangle$ under the adiabatic Hamiltonian only, with the CD driving H_1 applied and with H_1' applied, respectively. The average energy for the adiabatic Hamiltonian $H_{\text{tot}} = H_{\text{r}}$ is higher than that with the CD driving H_1 or H_1', indicating nonzero diabatic transition to the excited states, while the average energy with the CD driving H_1 is the same as that with H_1', confirming that these two CD Hamiltonians give the same dynamics. In Fig. 7(d) we plot the energy cost ΔE vs the time t/T. For the adiabatic process under the Hamiltonian $H_{\text{tot}} = H_{\text{r}}$, $\Delta E = 0$ at time $t = 0$, because the initial state is the ground state of the instantaneous Hamiltonian. During the evolution, ΔE continuously increases due to the diabatic transition to the excited state. Under the CD driving H_1 or H_1', the energy cost is nonzero. This is because the state $v(t)$ at an arbitrary time t is the instantaneous ground state of H_{r} but not the ground state of the total Hamiltonian with the CD driving H_1 or H_1' being nonzero at any time t including the initial and the final times.

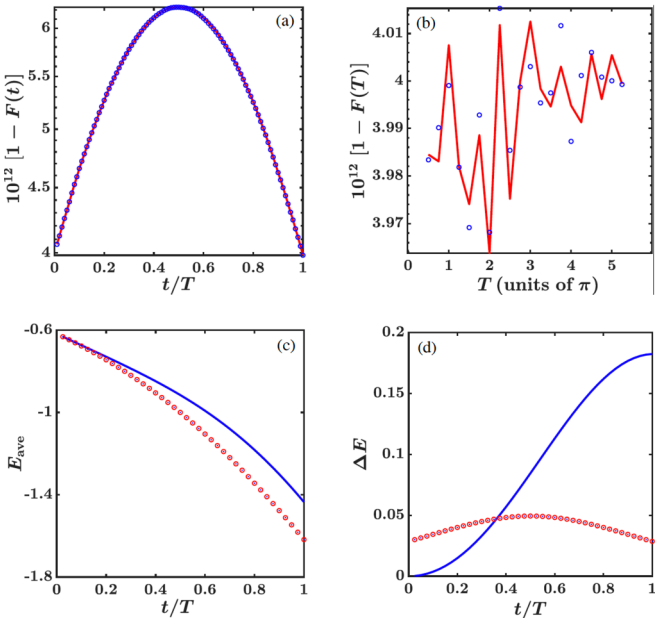

FIG. 7. (a) Infidelity $1 - F(t)$ vs t/T for total evolution time $T = 0.5\pi$. (b) Infidelity $1 - F(T)$ vs T. In (a) and (b) the red solid line (blue circles) represents under the adiabatic Hamiltonian H_{r} with the CD driving H_1 (H_1') applied. (c) Average energy E_{ave} vs t/T. (d) Energy cost ΔE vs t/T. In (c) and (d) the blue solid line represents under H_{r} only, red circles represent with H_1 applied, and blue dots are with H_1' applied. All the plots are for two sites, one excitation with linear ramping of J, and the parameters are given in Fig. 3 in dimensionless unit.

APPENDIX B: CD DRIVING FOR TWO EXCITATIONS

For a two-site lattice with two polariton excitations, the adiabatic Hamiltonian is given in Eq. (14). Solving this Hamiltonian for $\Delta = 0$, we can find its eigenvalues and eigenvectors. The eigenvalues are given in (15) and the eigenvectors are

$$|v_1\rangle = (0, -JA_1, 0, -JA_1, -gA_1, 0, 0, 1),$$

$$|v_2\rangle = (A_2, 0, -A_2, 0, 0, -1, 1, 0),$$

$$|v_{3,4}\rangle = \left(-\frac{1}{A_2}, \pm\frac{1}{A_3}, \frac{1}{A_2}, \mp\frac{1}{A_3}, 0, -1, 1, 0\right),$$

$$|v_{5,6}\rangle = (\pm X_-, Y_-, \pm X_-, Y_-, Z_-, \pm M_-, \pm M_-, 1),$$

$$|v_{7,8}\rangle = (\mp X_+, Y_+, \mp X_+, Y_+, Z_+, \mp M_+, \mp M_+, 1),$$

where we define

$$A_1 = \frac{g}{g^2 - J^2}, \quad A_2 = -\frac{J}{\sqrt{2}g}, \quad A_3 = -\frac{J}{\sqrt{2g^2 + J^2}}, \quad A_4 = \sqrt{4g^4 + 60g^2J^2 + 9J^4},$$

$$X_\pm = -\frac{24J}{g^2}\frac{[\pm 2g^6 + g^4(\pm 19J^2 + A_4) + J^4(\pm 3J^2 + A_4) + g^2(\pm 19J^4 + 3J^2A_4)]}{\sqrt{6g^2 + 5J^2 \pm A_4}(\pm 2g^2 \pm 9J^2 + A_4)(\pm 2g^2 \pm 3J^2 + A_4)},$$

$$Y_\pm = -\frac{8J}{g}\frac{[16g^6 + g^4(166J^2 \pm 8A_4) \pm 12J^4(\pm 3J^2 + A_4) + g^2(201J^4 \pm 29J^2A_4)]}{(2g^2 + 3J^2 \pm A_4)(6g^2 + 5J^2 \pm A_4)(2g^2 + 9J^2 \pm A_4)},$$

$$Z_\pm = \frac{2}{g^2}\frac{[8g^6 + g^4(90J^2 \pm 4A_4) \pm 8J^4(3J^2 + A_4) + g^2(125J^4 \pm 17J^2A_4)]}{(\pm 2g^2 \pm 9J^2 + A_4)(\pm 6g^2 \pm 5J^2 + A_4)},$$

$$M_\pm = \frac{2\sqrt{2}}{g}\frac{[\pm 2g^4 + g^2(\pm 11J^2 + A_4) + J^2(\pm 3J^2 + A_4)]}{(2g^2 + 3J^2 \pm A_4)\sqrt{6g^2 + 5J^2 \pm A_4}}.$$

Note that the eigenvectors given above have not been normalized. We find that the eigenvectors can be grouped into two subsets. The first subset is composed of the antisymmetric eigenvectors $\{v_2, v_3, v_4\}$ and the second subset is composed of the symmetric eigenvectors $\{v_1, v_5, v_6, v_7, v_8\}$.

Using the expressions of the eigenvalues, eigenvectors, and Eq. (1), we can derive the CD driving H_1 for this system, but we cannot write H_1 in an analytical form, nor can we find an implementable CD driving as we did in Sec. III A for the case of one excitation. As varying the adiabatic Hamiltonian H_r only induces diabatic transitions between eigenstates of the same symmetry, the CD driving only contains nonzero matrix elements between eigenstates in the same subset. We find that when considering only the matrix elements for the first subset $\{v_2, v_3, v_4\}$, the CD Hamiltonian can be written in terms of the qubit and cavity operators as

$$H_1' = i\frac{g}{2(J^2 + 2g^2)}\frac{\partial J}{\partial t}[(a_1^\dagger)^2\sigma_{1-}a_2 - (a_1^\dagger)^2 a_1\sigma_{2-} - (a_2^\dagger)^2\sigma_{1-}a_2 + (a_2^\dagger)^2 a_1\sigma_{2-}] + \text{H.c.} \tag{B1}$$

Defining $A_2 = a_1^2 - a_2^2$ and $C_2 = a_2\sigma_{1-} - a_1\sigma_{2-}$, it can be shown that Eq. (B1) leads to Eq. (16) in Sec. III C. On the other hand, we cannot find an analytical expression for the CD driving for the second subset that contains the ground state v_7.

[1] T. Albash and D. A. Lidar, Adiabatic quantum computation, Rev. Mod. Phys. **90**, 015002 (2018).

[2] E. Farhi, J. Goldstone, S. Gutmann, J. Lapan, A. Lundgren, and D. Preda, A quantum adiabatic evolution algorithm applied to random instances of an NP-complete problem, Science **292**, 472 (2001).

[3] J. Preskill, Quantum computing in the NISQ era and beyond, Quantum **2**, 79 (2018).

[4] K. Bharti, A. Cervera-Lierta, T. H. Kyaw, T. Haug, S. Alperin-Lea, A. Anand, M. Degroote, H. Heimonen, J. S. Kottmann, T. Menke, W.-K. Mok, S. Sim, L.-C. Kwek, and A. Aspuru-Guzik, Noisy intermediate-scale quantum algorithms, Rev. Mod. Phys. **94**, 015004 (2022).

[5] D. Guéry-Odelin, A. Ruschhaupt, A. Kiely, E. Torrontegui, S. Martínez-Garaot, and J. G. Muga, Shortcuts to adiabaticity: Concepts, methods, and applications, Rev. Mod. Phys. **91**, 045001 (2019).

[6] M. Kolodrubetz, D. Sels, P. Mehta, and A. Polkovnikov, Geometry and non-adiabatic response in quantum and classical systems, Phys. Rep. **697**, 1 (2017).

[7] R. G. Unanyan, L. P. Yatsenko, K. Bergmann, and B. W. Shore, Laser-induced adiabatic atomic reorientation with control of diabatic losses, Opt. Commun. **139**, 48 (1997).

[8] A. Emmanouilidou, X.-G. Zhao, P. Ao, and Q. Niu, Steering an eigenstate to a destination, Phys. Rev. Lett. **85**, 1626 (2000).

[9] M. V. Berry, Transitionless quantum driving, J. Phys. A: Math. Theor. **42**, 365303 (2009).

[10] M. Demirplak and S. A. Rice, On the consistency, extremal, and global properties of counterdiabatic fields, J. Chem. Phys. **129**, 154111 (2008).

[11] X. Chen, I. Lizuain, A. Ruschhaupt, D. Guéry-Odelin, and J. G. Muga, Shortcut to adiabatic passage in two- and three-level atoms, Phys. Rev. Lett. **105**, 123003 (2010).

[12] A. del Campo, M. M. Rams, and W. H. Zurek, Assisted finite-rate adiabatic passage across a quantum critical point: Exact solution for the quantum Ising model, Phys. Rev. Lett. **109**, 115703 (2012).

[13] B. Damski, Counterdiabatic driving of the quantum Ising model, J. Stat. Mech. (2014) P12019.

[14] X. Chen, A. Ruschhaupt, S. Schmidt, A. del Campo, D. Guéry-Odelin, and J. G. Muga, Fast optimal frictionless atom cooling in harmonic traps: Shortcut to adiabaticity, Phys. Rev. Lett. **104**, 063002 (2010).

[15] J. Jing, L.-A. Wu, M. S. Sarandy, and J. G. Muga, Inverse engineering control in open quantum systems, Phys. Rev. A **88**, 053422 (2013).

[16] F. Motzoi, J. M. Gambetta, P. Rebentrost, and F. K. Wilhelm, Simple pulses for elimination of leakage in weakly nonlinear qubits, Phys. Rev. Lett. **103**, 110501 (2009).

[17] A. Baksic, H. Ribeiro, and A. A. Clerk, Speeding up adiabatic quantum state transfer by using dressed states, Phys. Rev. Lett. **116**, 230503 (2016).

[18] T. Wang, Z. Zhang, L. Xiang, Z. Jia, P. Duan, W. Cai, Z. Gong, Z. Zong, M. Wu, J. Wu, L. Sun, Y. Yin, and G. Guo, The

experimental realization of high-fidelity 'shortcut-to-adiabaticity' quantum gates in a superconducting Xmon qubit, New J. Phys. **20**, 065003 (2018).
[19] A. Vepsäläinen, S. Danilin, and G. S. Paraoanu, Optimal superadiabatic population transfer and gates by dynamical phase corrections, Quantum Sci. Technol. **3**, 024006 (2018).
[20] L. S. Theis, F. Motzoi, and F. K. Wilhelm, Simultaneous gates in frequency-crowded multilevel systems using fast, robust, analytic control shapes, Phys. Rev. A **93**, 012324 (2016).
[21] J. M. Martinis and M. R. Geller, Fast adiabatic qubit gates using only σ_z control, Phys. Rev. A **90**, 022307 (2014).
[22] T. Yan, B.-J. Liu, K. Xu, C. Song, S. Liu, Z. Zhang, H. Deng, Z. Yan, H. Rong, K. Huang, M.-H. Yung, Y. Chen, and D. Yu, Experimental realization of nonadiabatic shortcut to non-Abelian geometric gates, Phys. Rev. Lett. **122**, 080501 (2019).
[23] Z.-T. Liang, X. Yue, Q. Lv, Y.-X. Du, W. Huang, H. Yan, and S.-L. Zhu, Proposal for implementing universal superadiabatic geometric quantum gates in nitrogen-vacancy centers, Phys. Rev. A **93**, 040305(R) (2016).
[24] Y.-X. Du, Z.-T. Liang, Y.-C. Li, X.-X. Yue, Q.-X. Lv, W. Huang, X. Chen, H. Yan, and S.-L. Zhu, Experimental realization of stimulated Raman shortcut-to-adiabatic passage with cold atoms, Nat. Commun. **7**, 12479 (2016).
[25] B. B. Zhou, A. Baksic, H. Ribeiro, C. G. Yale, F. J. Heremans, P. C. Jerger, A. Auer, G. Burkard, A. A. Clerk, and D. D. Awschalom, Accelerated quantum control using superadiabatic dynamics in a solid-state lambda system, Nat. Phys. **13**, 330 (2017).
[26] S. Masuda, K. Y. Tan, and M. Nakahara, Spin-selective electron transfer in a quantum dot array, Phys. Rev. B **97**, 045418 (2018).
[27] M. G. Bason, M. Viteau, N. Malossi, P. Huillery, E. Arimondo, D. Ciampini, R. Fazio, V. Giovannetti, R. Mannella, and O. Morsch, High-fidelity quantum driving, Nat. Phys. **8**, 147 (2012).
[28] T. Hatomura, Shortcuts to adiabatic cat-state generation in bosonic Josephson junctions, New J. Phys. **20**, 015010 (2018).
[29] D. Stefanatos and E. Paspalakis, Maximizing entanglement in bosonic Josephson junctions using shortcuts to adiabaticity and optimal control, New J. Phys. **20**, 055009 (2018).
[30] J. Zhang, T. H. Kyaw, D. M. Tong, E. Sjöqvist, and L.-C. Kwek, Fast non-Abelian geometric gates via transitionless quantum driving, Sci. Rep. **5**, 18414 (2015).
[31] A. del Campo, Shortcuts to adiabaticity by counterdiabatic driving, Phys. Rev. Lett. **111**, 100502 (2013).
[32] S. Deffner, C. Jarzynski, and A. del Campo, Classical and quantum shortcuts to adiabaticity for scale-invariant driving, Phys. Rev. X **4**, 021013 (2014).
[33] D. Sels and A. Polkovnikov, Minimizing irreversible losses in quantum systems by local counterdiabatic driving, Proc. Natl. Acad. Sci. USA **114**, E3909 (2017).
[34] K. Takahashi, Shortcuts to adiabaticity for quantum annealing, Phys. Rev. A **95**, 012309 (2017).
[35] T. Opatrný and K. Mølmer, Partial suppression of nonadiabatic transitions, New J. Phys. **16**, 015025 (2014).
[36] E. Boyers, M. Pandey, D. K. Campbell, A. Polkovnikov, D. Sels, and A. O. Sushkov, Floquet-engineered quantum state manipulation in a noisy qubit, Phys. Rev. A **100**, 012341 (2019).
[37] P. W. Claeys, M. Pandey, D. Sels, and A. Polkovnikov, Floquet-engineering counterdiabatic protocols in quantum many-body systems, Phys. Rev. Lett. **123**, 090602 (2019).
[38] N. N. Hegade, X. Chen, and E. Solano, Digitized counterdiabatic quantum optimization, Phys. Rev. Res. **4**, L042030 (2022).
[39] C. Mc Keever and M. Lubasch, Towards adiabatic quantum computing using compressed quantum circuits, PRX Quantum **5**, 020362 (2024).
[40] I. Čepaitė, A. Polkovnikov, A. J. Daley, and C. W. Duncan, Counterdiabatic optimized local driving, PRX Quantum **4**, 010312 (2023).
[41] M. J. Hartmann, F. G. S. L. Brandão, and M. B. Plenio, Strongly interacting polaritons in coupled arrays of cavities, Nat. Phys. **2**, 849 (2006).
[42] A. D. Greentree, C. Tahan, J. H. Cole, and L. C. L. Hollenberg, Quantum phase transitions of light, Nat. Phys. **2**, 856 (2006).
[43] D. G. Angelakis, M. F. Santos, and S. Bose, Photon-blockade-induced Mott transitions and XY spin models in coupled cavity arrays, Phys. Rev. A **76**, 031805(R) (2007).
[44] D. Rossini and R. Fazio, Mott-insulating and glassy phases of polaritons in 1D arrays of coupled cavities, Phys. Rev. Lett. **99**, 186401 (2007).
[45] N. Na, S. Utsunomiya, L. Tian, and Y. Yamamoto, Strongly correlated polaritons in a two-dimensional array of photonic crystal microcavities, Phys. Rev. A **77**, 031803(R) (2008).
[46] J. Koch and K. Le Hur, Superfluid–Mott-insulator transition of light in the Jaynes-Cummings lattice, Phys. Rev. A **80**, 023811 (2009).
[47] K. Seo and L. Tian, Quantum phase transition in a multiconnected superconducting Jaynes-Cummings lattice, Phys. Rev. B **91**, 195439 (2015).
[48] J. Xue, K. Seo, L. Tian, and T. Xiang, Quantum phase transition in a multiconnected Jaynes-Cummings lattice, Phys. Rev. B **96**, 174502 (2017).
[49] C. Noh and D. G. Angelakis, Quantum simulations and many-body physics with light, Rep. Prog. Phys. **80**, 016401 (2017).
[50] A. A. Houck, H. E. Türeci, and J. Koch, On-chip quantum simulation with superconducting circuits, Nat. Phys. **8**, 292 (2012).
[51] A. J. Hoffman, S. J. Srinivasan, S. Schmidt, L. Spietz, J. Aumentado, H. E. Türeci, and A. A. Houck, Dispersive photon blockade in a superconducting circuit, Phys. Rev. Lett. **107**, 053602 (2011).
[52] V. G. Sala, D. D. Solnyshkov, I. Carusotto, T. Jacqmin, A. Lemaître, H. Terças, A. Nalitov, M. Abbarchi, E. Galopin, I. Sagnes, J. Bloch, G. Malpuech, and A. Amo, Spin-orbit coupling for photons and polaritons in microstructures, Phys. Rev. X **5**, 011034 (2015).
[53] G. Lepert, M. Trupke, M. J. Hartmann, M. B. Plenio, and E. A. Hinds, Arrays of waveguide-coupled optical cavities that interact strongly with atoms, New J. Phys. **13**, 113002 (2011).
[54] P. A. Ivanov, S. S. Ivanov, N. V. Vitanov, A. Mering, M. Fleischhauer, and K. Singer, Simulation of a quantum phase transition of polaritons with trapped ions, Phys. Rev. A **80**, 060301(R) (2009).
[55] K. Toyoda, Y. Matsuno, A. Noguchi, S. Haze, and S. Urabe, Experimental realization of a quantum phase transition of polaritonic excitations, Phys. Rev. Lett. **111**, 160501 (2013).
[56] S. Debnath, N. M. Linke, S.-T. Wang, C. Figgatt, K. A. Landsman, L.-M. Duan, and C. Monroe, Observation of hopping and blockade of bosons in a trapped ion spin chain, Phys. Rev. Lett. **120**, 073001 (2018).

[57] B.-W. Li, Q.-X. Mei, Y.-K. Wu, M.-L. Cai, Y. Wang, L. Yao, Z.-C. Zhou, and L.-M. Duan, Observation of non-Markovian spin dynamics in a Jaynes-Cummings-Hubbard model using a trapped-ion quantum simulator, Phys. Rev. Lett. **129**, 140501 (2022).

[58] M. Fitzpatrick, N. M. Sundaresan, A. C. Y. Li, J. Koch, and A. A. Houck, Observation of a dissipative phase transition in a one-dimensional circuit QED lattice, Phys. Rev. X **7**, 011016 (2017).

[59] F. Nissen, S. Schmidt, M. Biondi, G. Blatter, H. E. Türeci, and J. Keeling, Nonequilibrium dynamics of coupled qubit-cavity arrays, Phys. Rev. Lett. **108**, 233603 (2012).

[60] J. Larson and T. Mavrogordatos, *The Jaynes-Cummings Model and Its Descendants: Modern Research Directions* (IOP, Bristol, 2021).

[61] Y. Hu and L. Tian, Deterministic generation of entangled photons in superconducting resonator arrays, Phys. Rev. Lett. **106**, 257002 (2011).

[62] K. Cai, P. Parajuli, G. Long, C. W. Wong, and L. Tian, Robust preparation of many-body ground states in Jaynes-Cummings lattices, npj Quantum Inf. **7**, 96 (2021).

[63] P. Parajuli, A. Govindarajan, and L. Tian, State preparation in a Jaynes-Cummings lattice with quantum optimal control, Sci. Rep. **13**, 19924 (2023).

[64] K. Funo, N. Lambert, and F. Nori, General bound on the performance of counter-diabatic driving acting on dissipative spin systems, Phys. Rev. Lett. **127**, 150401 (2021).

[65] S. Alipour, A. Chenu, A. T. Rezakhani, and A. del Campo, Shortcuts to adiabaticity in driven open quantum systems: Balanced gain and loss and non-Markovian evolution, Quantum **4**, 336 (2020).

[66] P. Krantz, M. Kjaergaard, F. Yan, T. P. Orlando, S. Gustavsson, and W. D. Oliver, A quantum engineer's guide to superconducting qubits, Appl. Phys. Rev. **6**, 021318 (2019).

[67] A. Blais, A. L. Grimsmo, S. M. Girvin, and A. Wallraff, Circuit quantum electrodynamics, Rev. Mod. Phys. **93**, 025005 (2021).

[68] B. K. Mitchell, R. K. Naik, A. Morvan, A. Hashim, J. M. Kreikebaum, B. Marinelli, W. Lavrijsen, K. Nowrouzi, D. I. Santiago, and I. Siddiqi, Hardware-efficient microwave-activated tunable coupling between superconducting qubits, Phys. Rev. Lett. **127**, 200502 (2021).

[69] D. L. Campbell, A. Kamal, L. Ranzani, M. Senatore, and M. D. LaHaye, Modular tunable coupler for superconducting circuits, Phys. Rev. Appl. **19**, 064043 (2023).

[70] Y. Chen, C. Neill, P. Roushan, N. Leung, M. Fang, R. Barends, J. Kelly, B. Campbell, Z. Chen, B. Chiaro, A. Dunsworth, E. Jeffrey, A. Megrant, J. Y. Mutus, P. J. J. O'Malley, C. M. Quintana, D. Sank, A. Vainsencher, J. Wenner, T. C. White *et al.*, Qubit architecture with high coherence and fast tunable coupling, Phys. Rev. Lett. **113**, 220502 (2014).

[71] F. Yan, P. Krantz, Y. Sung, M. Kjaergaard, D. L. Campbell, T. P. Orlando, S. Gustavsson, and W. D. Oliver, Tunable coupling scheme for implementing high-fidelity two-qubit gates, Phys. Rev. Appl. **10**, 054062 (2018).

[72] M. Sandberg, C. M. Wilson, F. Persson, T. Bauch, G. Johansson, V. Shumeiko, T. Duty, and P. Delsing, Tuning the field in a microwave resonator faster than the photon lifetime, Appl. Phys. Lett. **92**, 203501 (2008).

[73] K. Georgopoulos, C. Emary, and P. Zuliani, Modeling and simulating the noisy behavior of near-term quantum computers, Phys. Rev. A **104**, 062432 (2021).

[74] O. Abah and M. Paternostro Shortcut-to-adiabaticity Otto engine: A twist to finite-time thermodynamics, Phys. Rev. E **99**, 022110 (2019).

Correction: Support information was incomplete and has been fixed.